ESR spectrometer at 250GHz

Keith A. Earle and Jack H. Freed
Baker Laboratory of Chemistry
Cornell University
Ithaca, NY 14853-1301

ABSTRACT

We describe the design principles of an electron spin resonance (ESR) spectrometer operating at 250GHz, which uses quasioptics to propagate the far-infrared (FIR) radiation instead of conventional waveguide techniques. We include examples that illustrate the sensitivity and flexibility of the spectrometer. We also include a quasi-optical analysis of the expected performance of a novel reflection mode spectrometer.

keywords: far infrared, electron spin resonance, materials research, reflection spectroscopy, quasioptics

1 INTRODUCTION

Electron spin resonance (ESR) is a well-established experimental method that is used to study electron magnetic dipole transitions among energy levels that are split by a magnetic field. The EPR-active electrons may arise from crystalline defects, *e.g.* F-centers in irradiated quartz, paramagnetic impurities doped into a diamagnetic host,[1] or they may be incorporated in special molecules called spin probes. ESR spectroscopy of spin probes in fluid media has been a fruitful approach for elucidating the structure and dynamics of simple and complex fluids.[2–4]

ESR has conventionally been limited to 35GHz and lower in frequency. During the course of the last decade, a number of laboratories[5–9] developed instruments that have pushed the maximum observation frequency up to nearly 1THz (1000GHz). Pulse methods at frequencies up to 140GHz have also been developed,[10–12] as well as Electron Nuclear DOuble Resonance (ENDOR).[13]

The motivation for this intense activity is the resolution enhancement available from higher magnetic fields, which enables small but significant anisotropies in the ESR spectrum to be readily observed.[14] For systems with large level splittings in the absence of an applied magnetic field,[1] high-field spectra can be much simpler to analyze then X-band spectra, which increases the reliability and eases the interpretation of the data. In the study of fluid media,[4] ESR spectra of spin probes at X-band and 250GHz on the same system are sensitive to different interactions. In other words, the high-field spectra give information that is complementary to lower-field spectra. Combining studies at two or more frequencies provides a more stringent test for models of interactions in these systems and can lead to a deeper understanding of molecular processes in media of relevance to technology and medicine. These concepts are discussed more fully elsewhere,[2,3] and we refer the reader to the references for a more complete discussion.

Unlike conventional ESR spectrometers, the Cornell FIR-ESR spectrometer relies on quasioptics rather than

0-8194-1917-6/95/$6.00

fundamental mode waveguide to propagate the radiation. The Cornell 250GHz FIR-ESR spectrometer is shown in Figure 1. In several respects it is like a conventional ESR spectrometer in that it has a source, a resonator, detector, and it relies on magnetic field modulation to code the ESR signal for subsequent lock-in detection.

2 COMPONENTS

In this section we will discuss the considerations that influence the choice of source, detector, and magnet. Developments in source and detector technology, driven by applications in radar, communications, and radio astronomy, have been extremely important in the implementation of ESR spectroscopy at W-band (94GHz) and higher in frequency. The ready commercial availability of magnets of suitable homogeneity for high-resolution ESR work ($\approx 3 \times 10^{-6}$) for fields up to 9.5T has also been instrumental for exploiting the advances in source and detector technology at frequencies above Q-band.

The choice of magnetic field is important because it constrains the frequency of operation. Higher fields mean higher resolution in general, as in the case of Nuclear Magnetic Resonance (NMR), at least until the sources of inhomogeneous broadening, such as g-strain, broaden the line too severely. For systems that have g-values close to the free electron value, however, this is not a severe limitation. Current magnet technology sets a limit of 9.5T on the highest field that can be achieved at 4K without the use of advanced and expensive techniques. Given that field swept operation is still the most common mode of operation for high field spectrometers to date, the optimum magnet configuration involves a trade-off between sweepability versus homogeneity above 9.5T. Based on all these considerations, we may take 9.5T with a homogeneity of 3×10^{-6} as the upper limit of simple and economical operation. A magnetic field of 9.5T corresponds to a frequency of approximately 270GHz for a free electron. We operate at a slightly lower frequency so that we are not continually near the quench field of the magnet.

The Cornell spectrometer is based on a frequency tripled, phase-locked, cw, Gunn diode that has an output power of 3mW at 250GHz. The phase-lock circuitry is shown schematically in reference[7] and we will not comment on it further, except to note that the phase noise is -90dBc at an offset of 100kHz. The source is rugged, reliable, and very easy to use in practice. For detection, we use a GaAs whisker contact diode with a measured $NEP = 10^{-13}\mathrm{W}/\sqrt{\mathrm{Hz}}$ at a modulation frequency of 100kHz and a post-detection bandwidth of 1Hz. We will show in section 3 what implications this has for the minimum observable number of spins N_{min}.

A gaussian beam has a radial amplitude dependence $\exp -\rho^2/w^2(z)$ where

$$w(z) = w_0\sqrt{1+\left(\frac{z}{z_0}\right)^2}, \tag{1}$$

$z_0 = \pi w_0^2/\lambda$, the confocal distance, and λ is the radiation wavelength. It is easy to show from equation 1 that $\lim_{z\to\infty} w(z)/z = \lambda/\pi w_0$, the asymptote of a hyperbola. We call the quantity $\tan^{-1}(\lambda/\pi w_0)$ the asymptotic beam growth angle; for our system, it is approximately equal to 3°. The clear aperture of our magnet is 37.9mm, and we must propagate radiation over a distance of roughly 2m. In order to limit the growth of the beam, we use lenses to refocus the gaussian beam. For narrow-band systems, it is possible to design lenses that have extremely low reflection losses.[15] The insertion loss of the lenses that are used in the Cornell spectrometer, which includes losses in the lens material as well as reflection losses, is 0.1dB per lens.

A very useful and succinct discussion of optimizing lenses for transmission over relatively long distances is given by Goldsmith.[16] The basic result is that the maximum possible distance between two focusing elements for a Gaussian beam is twice the confocal distance, $d = 2z_0$, where $z_0 = kw_0^2/2$ and w_0 is the beam waist. In order to avoid truncating the beam, we require $a/w > 2$, where a is the lens aperture radius and w is the beam radius at the lens aperture. If we set $z = z_0$ in equation 1, we find $w(z_0) = \sqrt{2}w_0$ at the lens aperture. The distance d is therefore determined by quasioptical constraints to be $d \leq ka^2/8$, where $k = 2\pi/\lambda$. In terms of the aperture

diameter $D = 2a$, we find

$$d \leq \frac{\pi D^2}{16\lambda}. \tag{2}$$

The Cornell FIR-ESR spectrometer uses $D = 37.9$mm, $w_0 = 6.7$mm, $\lambda = 1.2$mm and $z_o = \pi w_0^2/\lambda = 117.5$mm, which results in $d = 235$mm. The focal length for the refocussing optics is $f = z_o$; the focal ratio $f/\# = 3$.

The FIR-ESR resonator is a semiconfocal resonator. For our purposes, it is important to note that in such a resonator, it is impossible to have an anti-node of the E field at the beam waist. The beam waist is given by the standard formula[17]

$$w_0^2 = \frac{\lambda}{\pi}\sqrt{d(R_0 - d)}, \tag{3}$$

where d is the mirror separation and R_0 is the spherical mirror radius of curvature. We operate near the confocal separation $R_0 = 2d = 25.4$mm, which implies that $w_0 \approx 2.2$mm in the resonator and that the longitudinal mode number $q \approx 20$. We choose such a small beam waist in order to concentrate the available power near the optical axis and enhance the ESR transition inducing rf magnetic field B_1 in the sample.

The sample Q, Q_χ, contains an EPR resonant contribution Q_{EPR}, and a non-resonant contribution $Q_{optical}$, which is determined by the optical properties of the sample: its thickness and index of refraction n. A slab of dielectric may be thought of as a Fabry-Pérot resonator (hence $Q_{optical}$). We may simply lump the non-resonant part of Q_χ, $Q_{optical}$ with Q_U, the unloaded Q of the resonator, and set $Q_\chi = Q_{EPR}$. The quantity Q_{EPR} is the source of the EPR signal. Off of EPR resonance Q_{EPR} is infinite because there is no absorption of the FIR field. On EPR resonance Q_{EPR} is finite due to FIR absorption. An expression for Q_L that incorporates these effects is:

$$\frac{1}{Q_L} = \left(\frac{1}{Q_U} + \frac{1}{Q_{optical}}\right) + \frac{1}{Q_R} + \frac{1}{Q_\chi}. \tag{4}$$

We may write $1/Q_\chi = \eta\chi''$ in equation 4 where η is the filling factor of the resonator (derived below), and χ'' is the absorptive part of the FIR susceptibility. Our resonator has a $Q_L \approx 200$.

In a resonator of high finesse, the presence of absorption not only broadens the resonator response, it also reduces the transmitted power. The optimum solution for studying lossy samples is to place them in regions of low E field in the resonator. We may model the coupling of the sample to the radiation in the resonator by computing the filling factor. The most straightforward way to accomplish this is to calculate the ratio of electromagnetic energy stored in the sample to the electromagnetic energy stored in the resonator. We may then use the result that the total energy in the resonator, representing the sum of the dielectric and air regions is

$$E_{total} = (1/8\pi)E_0^2 w_0^2(t\Delta + d), \tag{5}$$

where E_0 is the field strength in the resonator, t is the sample thickness, and Δ is a quasioptical correction to the thickness given by[18]

$$\Delta = n^2/[n^2\cos^2(nkt - \Phi_T) + \sin^2(nkt - \Phi_T)], \tag{6}$$

where Φ_T is a small phase correction that is two orders of magnitude smaller than nkt for thin or very thick ($t \approx d$) samples,[18] which are the two cases of greatest experimental interest. We will neglect Φ_T in the sequel. The filling factor may now be written down by inspection,

$$\eta = t\Delta/(t\Delta + d). \tag{7}$$

3 SPECTROMETER SENSITIVITY

The expression for the resonator Q in the presence of a sample may be found by defining the sample quality factor as the ratio of energy stored in the cavity to energy dissipated in the sample due to EPR absorption, which

may be related to the filling factor, η, and the rf susceptibility, χ'', *viz.* $Q_\chi = 1/\eta\chi''$. The fractional change in Q_L as on sweeps through the ESR resonance may be calculated from equation 4:

$$\Delta Q_L/Q_L = \frac{(Q_L)\,\chi''\eta}{1+(Q_L)\,\chi''\eta} \tag{8}$$

The change in rf voltage V_L at the detector, modelled by a load resistance R_L, due to a change in the loaded Q may be easily calculated from an equivalent lumped circuit for the resonator,[19] where the resonance absorption may be modelled as a change in the resonator inductive reactance. We find[19]

$$\frac{\Delta V_L}{\sqrt{R_L}} = \frac{V_L}{\sqrt{R_L}}\,(Q_L)\,\chi''\eta, \tag{9}$$

using equation 8 where we assume $\eta\chi'' \ll 1$.

The sensitivity limit corresponds to a signal to noise ratio of 1:1, which may be modelled by assuming a Johnson noise source at T_d of resistance R_L, where T_d may be calculated from the noise equivalent power of the detector, assuming that T_d has a $1/f_{mod}$ modulation frequency dependence. For a modulation frequency of 100kHz, we measure $T_d \approx 10^7$K. This should be compared to X-band detectors, which typically[20] have a noise temperature $\approx 10^3$K. FIR homodyne detectors are intrinsically noisier than their microwave frequency counterparts.

The sensitivity of a transmission mode spectrometer may be written as follows[19]

$$\begin{aligned} N_{min} \;=\; & \frac{3V_S k_B T_S (2S+1)}{g^2\beta_e^2 S(S+1)}\,\frac{\Delta H_{pp}}{H_0}\,\frac{\Delta H_{pp}}{H_{mod}} \\ & \times \frac{1}{\eta Q_L}\,\frac{(1+\beta_1+\beta_2)}{\sqrt{\beta_1\beta_2}}\left(\frac{k_B T_D \Delta f}{P_0}\right)^{1/2}, \end{aligned} \tag{10}$$

where V_S is the sample volume, T_S is the sample temperature, β_e is the Bohr magneton, ΔH_{pp} is the linewidth, H_0 is the Larmor field, H_{mod} is the modulation amplitude, k_B is Boltzmann's constant, the quantity $(2S+1)$ is the number of observed lines, β_1 and β_2 are the coupling parameters into and out of the resonator, T_D is the detector noise temperature, and Δf is the post-detection bandwidth.

Assuming a $g = 2$ system with a 1G linewidth at 8.9T using a 0.5mM sample near room temperature, a large filling factor $\eta \approx 1$, a sample volume approximately 0.5cm^3, $Q_L \approx 200$, a modulation amplitude $\approx \Delta H_{pp}/10$, coupling factors $\beta = \beta_1 = \beta_2 = .04$, a noise temperature $T_d \approx 10^7$K, a post-detection bandwidth of 1Hz and an FIR power of 3mW leads to $N_{min} \approx 10^{10}$. This corresponds to a motionally-narrowed nitroxide spin probe in a low-loss solvent. The experimentally observed $N_{min}^{(obs)} \approx 10^{11}$, which is comparable to the sensitivity of commercially available X-band spectrometers. Given the uncertainties in the various parameters as well as the neglect of the noise figure contribution from the post-detection chain, the agreement is satisfactory.

From equation 10 it is clear that their are several ways to reduce N_{min}. One can use a more powerful source, improve the coupling to the resonator, increase Q_L, use a detector with lower noise temperature, or all of the above. These points are covered more fully elsewhere,[19] and we refer the reader to this reference for a more complete analysis.

Figure 2 shows a set of spectra collected over three decades of the rotational diffusion rate. The system is the spin probe cholestane (CSL) in the organic glass *o*-terphenyl (OTP). The range of diffusion rates corresponds to the motional narrowing region with $R \approx 10^9$sec^{-1} at the top of the figure and the rigid limit with $R \approx 10^6$sec^{-1} at the bottom of the figure. Note the excellent signal to noise ratio. We have successfully varied the temperature of the spectrometer from -250C to 110C without compromising its performance.

We discuss in section 4 techniques for constructing a reflection mode spectrometer based on quasi-optical techniques. Assuming a critically coupled resonator in a reflection mode resonator, we estimate[19] a potential

reduction of N_{min} by a factor of 15dB over the optimum transmission mode spectrometer, or $N_{min}^{(Th)} = 6 \times 10^6$spins. This leads to a predicted *observable* N_{min} of about 6×10^7spins if we use the same scaling between the theoretical and observed N_{min} as above.

4 REFLECTION MODE SPECTROMETER

In this section, we will discuss a novel approach that will allow the spectrometer to be operated in the reflection mode, as shown in Figure 3. The most important element of the spectrometer in Figure 3 is the Polarization Transforming Reflector (PTR), which functions as a half wave plate in this configuration. In this configuration, the diplexer also isolates the source from the deleterious effects of back reflected power.

The advantage of quasioptical diplexing over ferrite or waveguide technology is that polarizers and other processing optics can be made with very low losses and high power handling capability. For example, wire grid polarizers transmit cross polarized radiation at levels of roughly -30dB or lower[21] and have an insertion loss of 0.1dB for the transmitted polarization. We see that polarization diplexing is very attractive in the near millimeter band. Furthermore, ferrite or waveguide-based components are not readily available above about 100GHz. We choose the Polarization Transforming Reflector (PTR) described by Howard[22] *et al.* as a practical implementation of diplexing via polarization coding.

The deviation of a practical device from the ideal response depends upon the ratio d/w, where d is the beam displacement within the PTR and w is the beam radius at the PTR. With an angle of incidence of 30° and a beam radius $w \approx 6\lambda$, it is possible to achieve $d/w \approx .02$ for a quarter wave plate, which we will take as a practical specification. The portion of the phase shifted beam in the fundamental may be used to calculate the polarization purity of the PTR output beam.[19] We may write

$$\begin{aligned} \mathbf{E}_r &\approx u_{00}\left(\hat{x} + ie^{-d^2/w^2}\hat{y}\right) \\ &= u_{00}\left(P_+(\hat{x} + i\hat{y}) + P_-(\hat{x} - i\hat{y})\right), \end{aligned} \tag{11}$$

where P_+ is the fraction of $\mathbf{E}_r$ that has positive helicity and P_- is the fraction of $\mathbf{E}_r$ that has negative helicity, u_{00} is fundamental gaussian beam mode of waist w_0, and

$$\frac{P_-}{P_+} = \tanh\left(\frac{d^2}{2w^2}\right), \tag{12}$$

which gives $20\log_{10}(P_-/P_+) \approx -70$dB for $d/w = .02$. The error terms due to imperfect beam overlap are essentially a power loss term and may be approximated[19] $P_{loss} \approx 20\log_{10}(d/w) = -34$dB. This calculation shows that it is practical to build a PTR which has an extremely pure polarization response and very low losses to higher order modes.

The measured performance of a PTR in the near millimeter band when used as a half-wave plate is discussed by Howard,[22] *et al.*; the polarization performance should be comparable to Howard's in the Cornell 250GHz spectrometer. The ultimate performance of the PTR depends on the ratio d/w which may be optimized by using an angle of incidence as small as practical and a beam waist as large as possible.

5 ADJUSTABLE FINESSE FABRY-PEROT RESONATOR

In order to optimize the performance of the resonator as samples of various sizes and loss tangents are studied, it is useful to have a means of varying the loaded Q of the resonator. As we discussed in section 3, a poorly coupled resonator reduces the highest achievable signal to noise ratio.

One approach is to use multiple mesh resonators, which are discussed by Garg and Pradhan[23] (and references therein). The advantage of using meshes instead of polarizers is that meshes have polarization independent response at normal incidence. As we discuss in the caption to Figure 3 it is desirable to use circular polarization to code the incident and reflected power. Treatments of wire meshes can be found in the book by Chantry[24] and in the chapters by Goldsmith[21] and Holah.[25] These treatments are based mainly on the original work of Ulrich[26] who derived an equivalent circuit analysis for wire meshes that works quite well in practice. Earle[19] *et al.* discuss in detail a novel resonator which uses a variable finesse planar Fabry-Pérot interferometer to vary the coupling into and out of the sample resonator, shown in Figure 4.

6 SUMMARY

We have now presented a description of the Cornell 250GHz spectrometer which uses quasi-optical techniques. We have also performed an analysis of the predicted performance of a novel reflection mode spectrometer with variable input coupling and transmit/receive diplexing based on polarization coding that will give significant improvements in the signal to noise. At every stage we have chosen parameters that correspond to practical performance values and measured response.

7 ACKNOWLEDGEMENTS

This work was supported by NIH grant RR07126, and NSF grant CHE9313167. KAE thanks professors P. F. Goldsmith, R. Compton, and M. Wengler for many useful discussions.

8 REFERENCES

[1] W. Bryan Lynch, R. Samuel Boorse, and Jack H. Freed. *JACS*, **115**, 10909–10915, 1993.

[2] Ya. Lebedev. *High-Frequency Continuous-Wave Electron Spin Resonance.* In L. Kevan and M. Bowman, editors, *Modern Pulsed and Continuous-Wave Electron Spin Resonance*, chapter 8. Wiley, 1990.

[3] D. E. Budil, K. A. Earle W. B. Lynch, and J. H. Freed. *Electron Paramagnetic Resonance at 1 Millimeter Wavelengths.* In A. J. Hoff, editor, *Advanced EPR: Applications in Biology and Biochemistry*, chapter 8. Elsevier, 1989.

[4] K. A. Earle, D. E. Budil, and J. H. Freed. *Journal of Physical Chemistry*, **97**, 13289–13297, 1993.

[5] O. Ya. Grinberg, A. A. Dubinskii, and Ya. S. Lebedev. *Russian Chemical Reviews*, **52**, 850, 1983.

[6] E. Haindl, K. Möbius, and H. Oloff. *Zeitschrift für Naturforschung*, **40a**, 169, 1985.

[7] W. B. Lynch, K. A. Earle, and J. H. Freed. *Rev. Sci. Inst.* **59**, 1345-1351, 1988.

[8] A. L. Barra, L.-C. Brunel, and J. B. Robert. *Chem. Phys. Lett.*, **165**, 107, 1990.

[9] W. Wang, R. L. Belford, R. B. Clarkson, P. H. Davis, J. Forrer, M. J. Nilges, M. D. Timken, T. Walczak, M. C. Thurnauer, J. R. Norris, A. L. Morris, and Y. Zhang. *Applied Magnetic Resonance*, **6**, 195–215, 1994.

[10] R. T. Weber, J. A. J. M. Disselhorst, L. J. Prevo, J. Schmidt, and W. Th. Wenckebach. *Journal of Magnetic Resonance*, **81**, 129–144, 1989.

[11] A. Yu. Bresgunov, A. A. Dubinskii, V. N. Krimov, Yu. G. Petrov, O. G. Poluektov, and Ya. S. Lebedev. *Applied Magnetic Resonance*, 2, 715, 1991.

[12] T. F. Prisner, S. Un, and R. G. Griffin. Pulsed ESR at 140GHz. *Israel Journal of Chemistry*, 32:357–363, 1992.

[13] O. Burghaus, A. Toth-Kischkat, R. Klette, and K. Möbius. *Journal of Magnetic Resonance*, **80**, 383–385, 1988.

[14] K. A. Earle, J. K. Moscicki, M. Ge, D. E. Budil, and J. H. Freed. *Biophysical Journal*, **66**, 1213–1221, 1994.

[15] R. Padman. *IEEE Transactions* **AP-26** 741, 1979.

[16] P. F. Goldsmith. *IEEE Proc.* **80** 1729-1747, 1992.

[17] H. Kogelnik and T. Li. *Appl. Optics* **5**, 1550-1567, 1966.

[18] P. K. Yu and A. L. Cullen. *Proc. Roy. Soc. Lond. A* **390**, 49-71, 1982.

[19] K. A. Earle, D. E. Budil, and J. H. Freed. Electron Spin Resonance at 250GHz Using Quasioptical Techniques. In W. Warren, editor, *Advances in Magnetic and Optical Resonance*. Academic, 1995. in press.

[20] A. Abragam and B. Bleaney. *Electron Paramagnetic Resonance of Transition Ions*, pages 125–132. Oxford, 1970.

[21] Paul Goldsmith. *Quasi-Optical Techniques at Millimeter and Submillimeter Wavelengths.* In Kenneth J. Button, editor, *Infrared and Millimeter Waves: Systems and Components*, volume 6. Academic, 1982.

[22] J. Howard, W. A. Peebles, and N. C. Luhmann, Jr. *International Journal of Infrared and Millimeter Waves* **7**, 1591-1603, 1986.

[23] R. K. Garg and M. M. Pradhan. *Infrared Physics* **18**, 292-298, 1978.

[24] G. W. Chantry. *Long-wave Optics.* Academic, 1984. vv. 1 and 2.

[25] G. D. Holah. *Far-Infrared and Submillimeter Wavelength Filters.* In K. Button, editor, *Infrared and Millimeter Waves: Systems and Components*, volume 6, chapter 6. Academic, 1982.

[26] R. Ulrich. *Infrared Physics* **19** 599, 1979.

Table 1: Legend for figure 1

A	9 Tesla magnet and sweep coils
B	phase-locked 250 GHz source
C	100 MHz master oscillator
D	Schottky diode detector
E	resonator and mod coils
F	250 GHz quasi-optical waveguide
G	power supply for main coil (100 A)
H	current ramp control for main magnet
I	power supply for sweep coil (50 A)
J	PC spectrometer controller
K	lock-in amp for signal
L	field-mod and lock-in reference
M	Fabry-Pérot tuning screw
N	vapor cooled leads for main solenoid
O	vapor cooled leads for sweep coil
P	^{4}He bath level indicator
Q	^{4}He transfer tube
R	bath temperature thermometer
S	^{4}He blow-off valves.

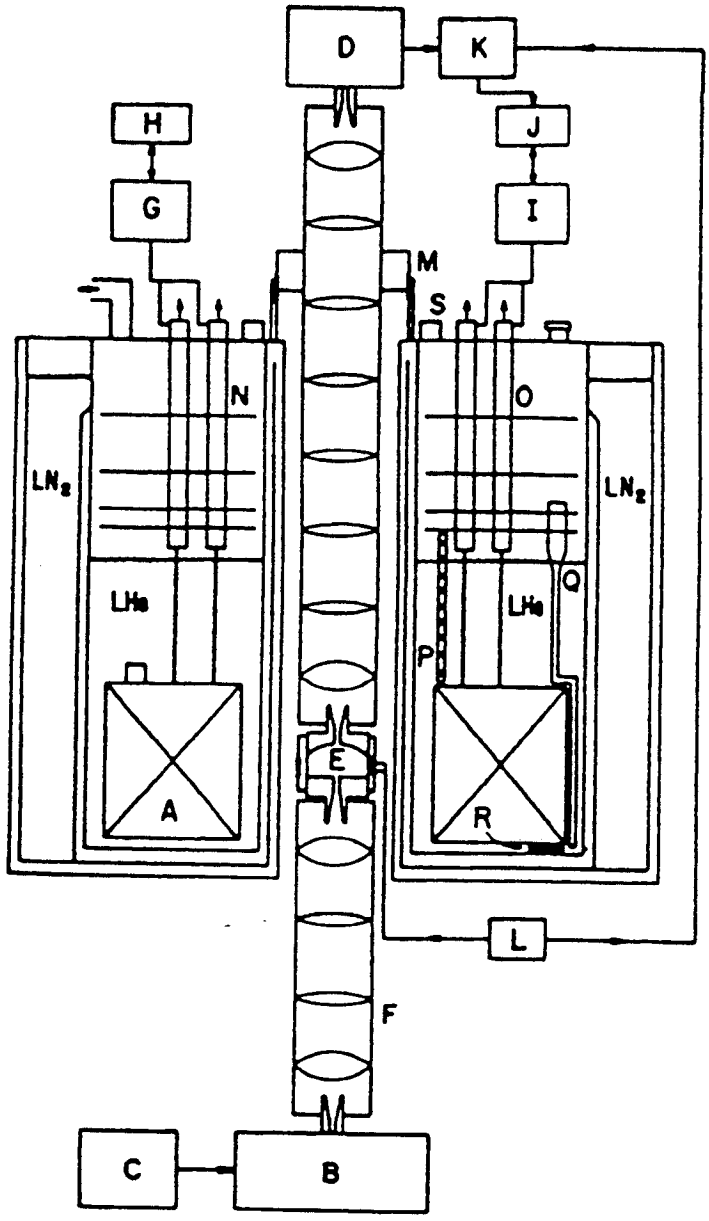

Figure 1: 249.9GHz FIR-ESR Spectrometer. Table 1 explains the meaning of the various symbols.

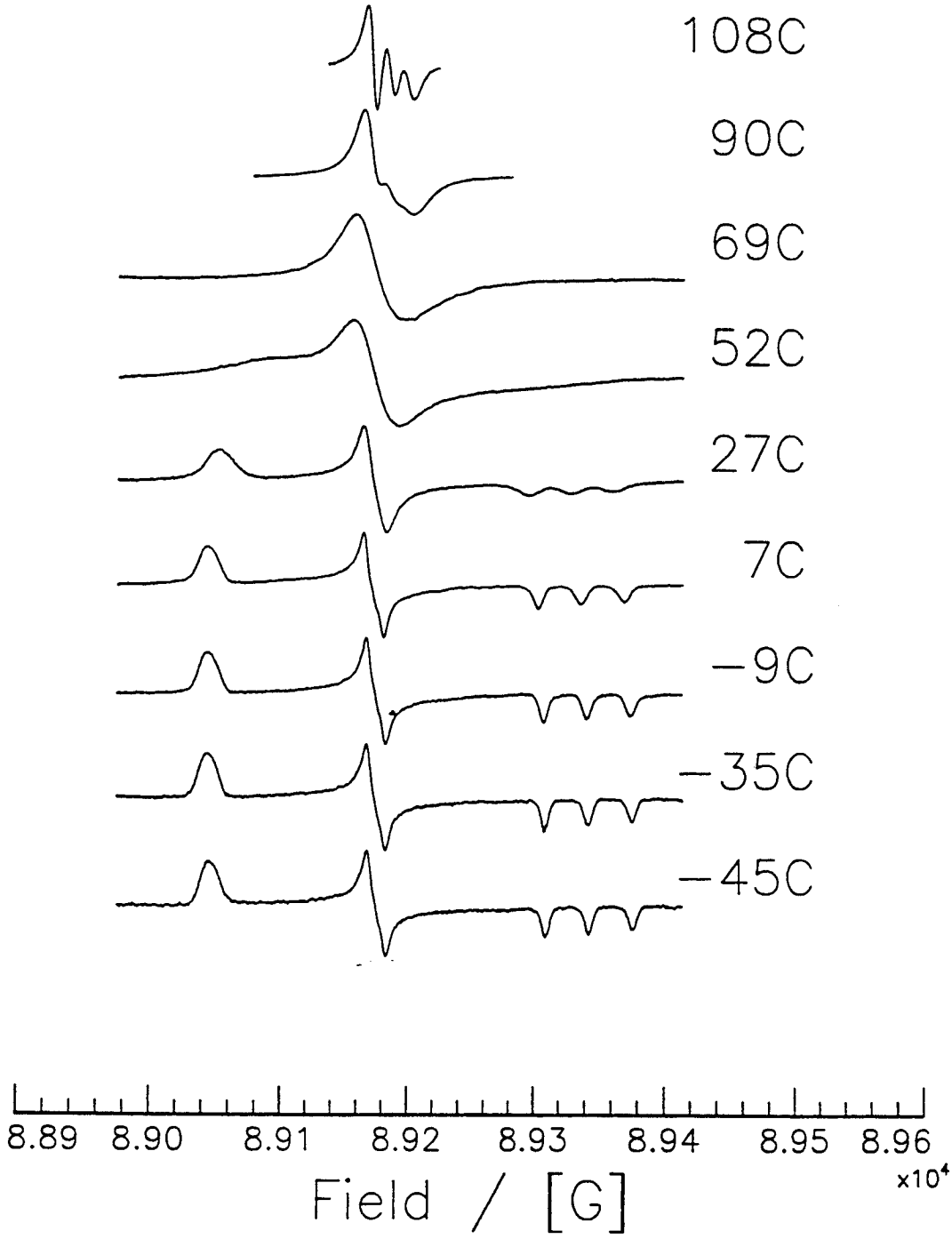

Figure 2: Complete motional range of the cholestane spin probe CSL in the organic glass o-terphenyl OTP. Note the excellent S/N.

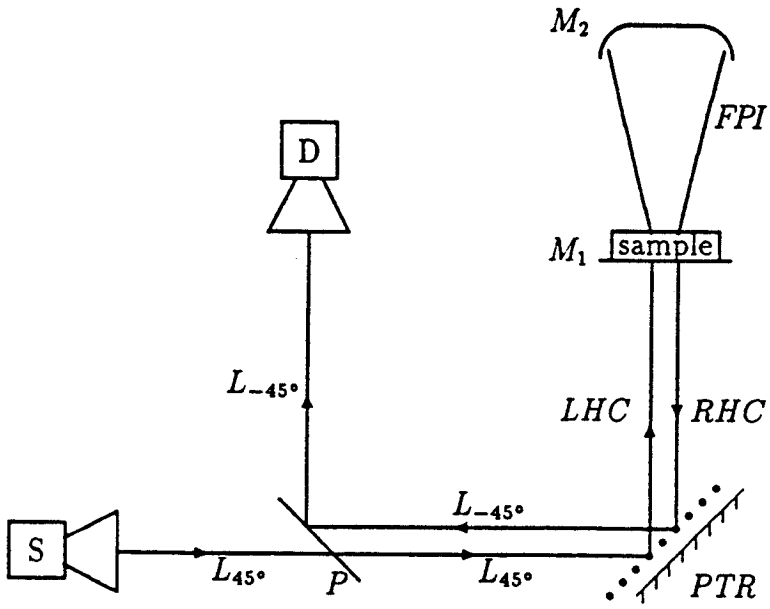

Figure 3: This figure shows a proposed optical layout for a reflection mode spectrometer with polarization coded diplexing. Polarizer P passes radiation linearly polarized at 45° ($L_{45°}$) with respect to the normal to the plane of the page. The Polarization Transforming Reflector PTR converts linearly polarized light to left hand circularly (LHC) polarized light. Upon reflection from the Fabry-Pérot Interferometer (FPI), the radiation is right hand circularly (RHC) polarized. After the second pass through the PTR, the polarization vector is rotated by 90° with respect to the incident radiation $L_{-45°}$. This polarization state is reflected by polarizer P into the detector D. The diverging lines in the FPI indicate the presence of diffractive beam growth that is controlled by the curved mirror M_2. The reflectivity of M_1 may be varied to adjust the coupling into and out of the FPI as discussed in the text.

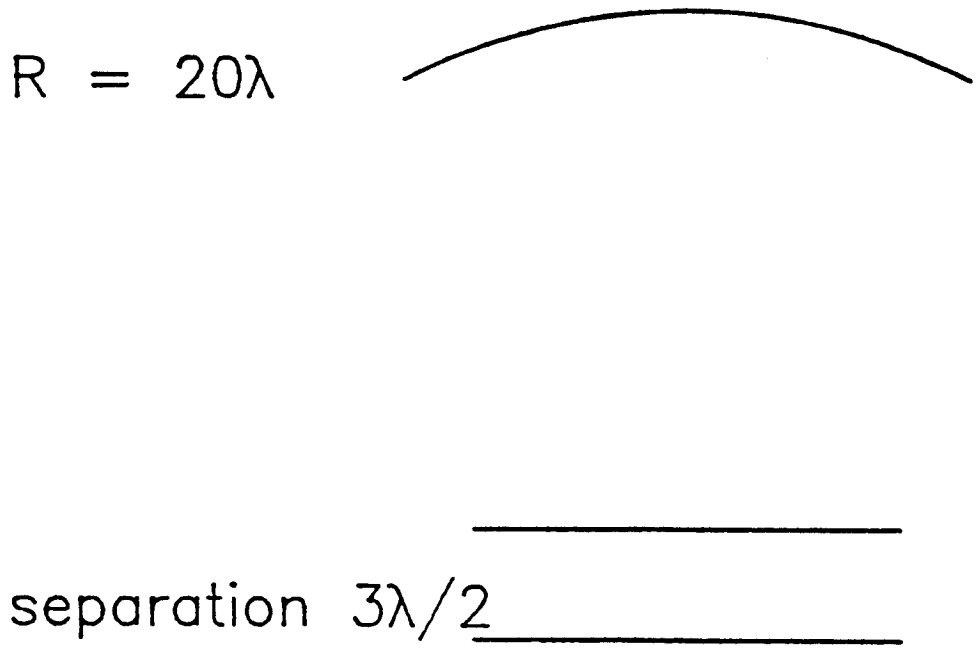

Figure 4: Schematic of a variable-coupling semiconfocal Fabry-Perot sample cavity. Varying the separation of the two wire meshes changes the apparent reflectivity of the planer Fabry-Pérot interferometer. The curved mirror refocuses the radiation.